Applied Physics Letters

RESEARCH ARTICLE | SEPTEMBER 28 2023

Ionization coefficients and excess noise characteristics of AlInAsSb on an InP substrate

T. J. Ronningen ; S. H. Kodati; X. Jin ; S. Lee ; H. Jung; X. Tao ; H. I. J. Lewis ; M. Schwartz ; N. Gajowski ; P. Martyniuk ; B. Guo ; A. H. Jones ; J. C. Campbell ; C. Grein ; J. P. R. David ; S. Krishna

Appl. Phys. Lett. 123, 131110 (2023)
https://doi.org/10.1063/5.0165800

AIP Publishing

Applied Physics Letters ARTICLE pubs.aip.org/aip/apl

Ionization coefficients and excess noise characteristics of AlInAsSb on an InP substrate

Cite as: Appl. Phys. Lett. **123**, 131110 (2023); doi: 10.1063/5.0165800
Submitted: 30 June 2023 · Accepted: 11 September 2023 ·
Published Online: 28 September 2023

T. J. Ronningen,[1] S. H. Kodati,[1] X. Jin,[2] S. Lee,[1] H. Jung,[1] X. Tao,[2] H. I. J. Lewis,[2] M. Schwartz,[1] N. Gajowski,[1] P. Martyniuk,[3] B. Guo,[4] A. H. Jones,[4] J. C. Campbell,[4] C. Grein,[5] J. P. R. David,[2] and S. Krishna[1,a)]

AFFILIATIONS

[1]Department of Electrical and Computer Engineering, The Ohio State University, Columbus, Ohio 43210, USA
[2]Department of Electronic and Electrical Engineering, The University of Sheffield, Sheffield S1 3JD, United Kingdom
[3]Institute of Applied Physics, Military University of Technology, Warsaw, Poland
[4]Department of Electrical and Computer Engineering, University of Virginia, Charlottesville, Virginia 22904, USA
[5]Department of Physics, University of Illinois, Chicago, Illinois 60607, USA

[a)]**Author to whom correspondence should be addressed:** krishna.53@osu.edu

ABSTRACT

For short-wavelength infrared (SWIR) avalanche photodiodes, a separate absorption, charge, and multiplication design is widely used. AlInAsSb on an InP substrate is a potential multiplication layer with a lattice match to absorber candidates across the SWIR. Our new measurements demonstrate that AlInAsSb on InP is a promising multiplier candidate with a relatively low dark current density of 10^{-4} A/cm^2 at a gain of 30; a high gain, measured up to 245 in this study; and a large differentiation of electron and hole ionization leading to a low excess noise, measured to be 2.5 at a gain of 30. These characteristics are all improvements over commercially available SWIR detectors incorporating InAlAs or InP as the multiplier. We measured and analyzed gain for multiple wavelengths to extract the ionization coefficients as a function of an electric field over the range 0.33–0.6 MV/cm.

An avalanche photodiode (APD) is a crucial component for low-light optical receivers. APDs targeting short-wavelength infrared (SWIR), especially 1.55 and 2 μm, have demonstrated promise for lidar applications in defense, space,[1,2] and commercial[3–5] sectors. APDs are particularly advantageous in low-light applications, because impact ionization increases the signal and can overcome circuit readout noise. The sensitivity of commercial APDs at 1.55 and 2 μm are limited primarily by their large excess noise, which limits the gain they can operate at. The sensitivity of an optical receiver is characterized by its signal to noise ratio (SNR). For an APD receiver with gain, SNR is given by[6]

$$SNR = \frac{I_{ph}^2 M^2}{2qM^2(I_{ph} + I_d)F(M)\Delta f + N_{Amp}}. \quad (1)$$

Here, I_{ph} is the gain-free photocurrent that is proportional to quantum efficiency (QE), M is the field-dependent gain from impact ionization, q is the elementary charge, I_d is the gain-free dark current, $F(M)$ is the excess noise factor, Δf is the bandwidth, and N_{amp} is the noise power from the readout circuit. The key to reduction of $F(M)$ at high gain is a multiplier material with a low k, the ratio of impact ionization coefficients of the holes (β) to electrons (α) (for an electron APD).[7–11] Therefore, for a given N_{amp}, a high QE, a low I_{d}, and a low k are all needed to increase the SNR of an APD. This study builds on a previous report[12] of these key characteristics for AlInAsSb on InP, measures a higher M and lower k than previously reported, extracts the material's ionization coefficients from measurements of gain close to breakdown, and demonstrates its promise as an APD multiplier.

A separate absorption, charge, and multiplication (SACM) APD design combines distinct materials for the absorption and multiplication stages. This enables the optimization of QE in the absorption layer and the optimization of M and k in the multiplication layer. For infrared APD applications, HgCdTe is an established, high performing APD technology[2,13] that is typically operated at 110 K or lower. Current commercial options for room temperature SWIR APDs are SACMs with absorber/multiplier pairs of InGaAs/InP and InGaAs/InAlAs.[14] These commercial options use an InP substrate to improve their manufacturability. The performance of these commercial options

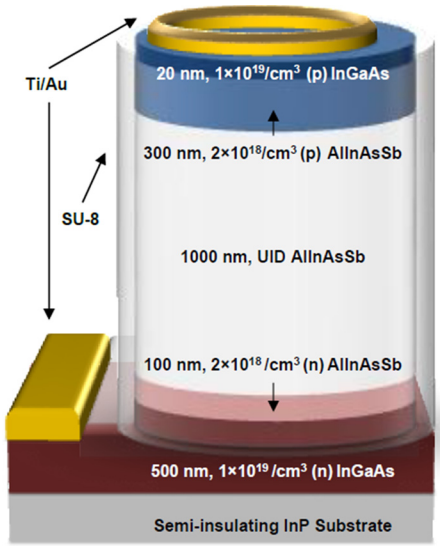

FIG. 1. Heterostructure and test device schematic for the PIN AlInAsSb test devices.

is limited by a high k value[15–20] in the multiplier that limits the operational gain and SNR. Researchers have identified several alternative, InP substrate-based multipliers (InAlAs,[21,22] AlAsSb,[23,24] AlGaAsSb,[25–27] AlGaInAs,[28] and now AlInAsSb) that improve k over InP or InAlAs.

An alloy of $Al_{0.70}In_{0.30}As_{0.74}Sb_{0.26}$ was grown as a random alloy on InP using molecular beam epitaxy as previously reported.[12,29] The schematic of the AlInAsSb PIN heterostructure and test device are shown in Fig. 1, and additional material characterization information is provided as the supplementary material. The 1000 nm unintentionally doped (UID) AlInAsSb layer is thick enough to ensure significant variations in the optical injection profile over the range of test wavelengths. A three-step fabrication procedure was employed to make single-pixel devices. In step 1, mesas were etched with a solution of citric acid (40 ml of 1 g:1 ml)/H_3PO_4 (10 ml)/H_2O_2 (10 ml)/H_2O (200 ml). In step 2, the wafer was dipped in HCl:H_2O (1:10) for 30 s to remove the native oxide and then passivated with SU-8 6000.5 (∼500 nm). In step 3, the wafer was again dipped in HCl:H_2O (1:10) for 30 s and then metalized with Ti/Au (12/150 nm) for the top and bottom contacts. The forward-bias current was measured to assess and verify that the series resistance was sufficiently low. The new fabrication led to a factor of 350 reduction in the series resistance (analysis provided in the supplementary material), and this enabled a more accurate analysis of the gain. Gain measurements [Fig. 2(a)] were made at the Ohio State University and the University of Sheffield. At gains up to 10, the measured gains agree within the precision established by device-to-device variation and analysis of the gain-free photocurrent correction. Above a gain of 10, the Ohio State gain results increased more quickly with bias [Fig. 2(a) inset]. This is attributed to a lower photon flux, and only the Ohio State gain results were used in subsequent analysis. Ohio State measured DC currents using a source-meter unit under dark [Fig. 2(b)] and illuminated (focused diode lasers) conditions. To calculate the gain accurately, it is good practice to account for the photocurrent increase that results from the increasing depletion width with voltage [Fig. 2(d)]. For this material, the increase in the depletion width is small relative to the depletion width, and the effect is estimated with a linear correction based on a fit to the low-voltage region.

These wavelength- and photon flux-dependent gain measurements, Fig. 2(a), of this structure determined that the previously reported[12] gain and noise characteristics were limited by the measurement conditions and not by the material. Photo-generated carriers can screen the applied electric field due to space charge effects,[30] and this has the consequence of suppressing gain with increasing photon flux. The maximum stable gain observed was 245 at a voltage of 59.1 V

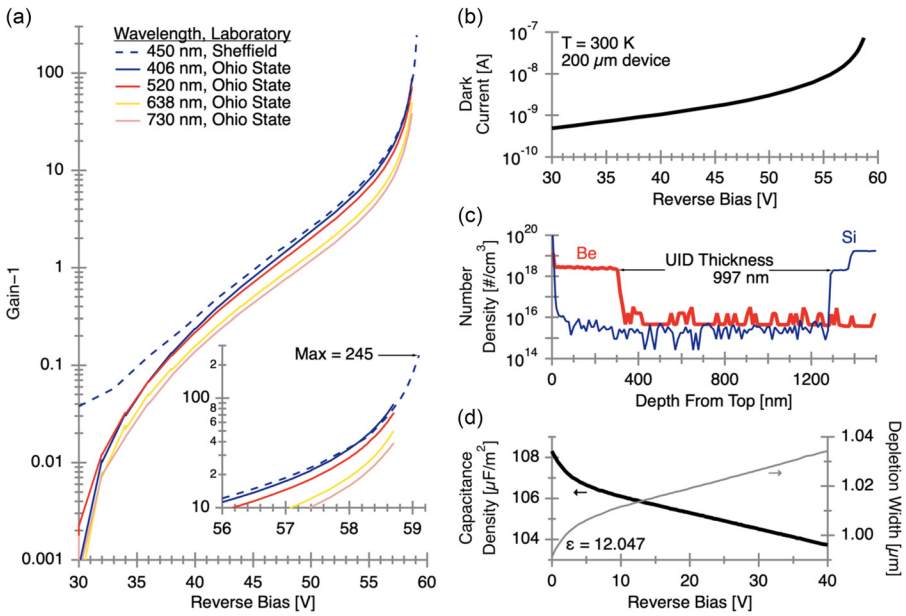

FIG. 2. (a) Gain vs reverse bias for five excitation wavelengths. The inset focuses on the gain above 56 V. Measurements were made at both Ohio State and Sheffield. The divergence of the Ohio State and Sheffield measurements at low voltage is a result of the depletion width correction applied. (b) Measured dark current for a 200 μm device. (c) SIMS measurement of the concentration of Be (p-dopant) and Si (n-dopant) as a function of the thickness of the PIN AlInAsSb. (d) CV measurement and calculated depletion width of a 250 μm diameter AlInAsSb device with a linearly decreasing capacitance above a 10 V bias.

with an excitation wavelength of 450 nm. The maximum observed gain was previously reported at 15,[12] but this limited gain is now believed to be due to this photon flux effect. For these AlInAsSb devices, the maximum gain for a given wavelength was observed when the unity gain photocurrent was less than 50 nA (1 to 50 μW optical power, dependent on wavelength), and the maximum gain did not increase at photocurrents below this. Figure 2(b) shows the dark current of the improved devices. An analysis of this dark current against single carrier gain finds that the bulk dark current density is 2.80 μA/cm^2 at unity gain and the surface dark current linear density is 2.7 nA/cm; a factor of 2 and 30 improvement, respectively, over the previous devices[12] (analysis provided in the supplementary material). With data from these improved devices and measurements, we applied a mixed injection approach to quantify the field dependence of the multiplier's impact ionization coefficients.

Avalanche gain is a consequence of carriers initiating impact ionization as they travel through the multiplier. The gain is both field- and position-dependent. The field dependence is captured in the depletion width (w), α, and β. The position dependence is then[6]

$$M(x) = \frac{(\alpha - \beta)e^{-(\alpha-\beta)x}}{\alpha e^{-(\alpha-\beta)w} - \beta}. \tag{2}$$

In single carrier injection, all photo-generated carriers are generated prior to entering the multiplication region. In mixed injection, carriers are also photo-generated in the multiplier region. The observed, average gain is then dependent on the carrier generation function, $G(x)$, as

$$\langle \mathrm{M} \rangle = \frac{\int_0^w M(x)G(x)dx}{\int_0^w G(x)dx}. \tag{3}$$

For the PIN devices in this study, the carriers are generated by photon absorption (G_a) with an exponential decay profile dependent on the absorption coefficient (γ_λ),

$$G_a(x) \propto e^{-\gamma_\lambda x}. \tag{4}$$

Sheffield has previously implemented a randomly generated ionization path length (RPL) model to analyze mixed injection data.[31] The RPL model uses the α, β, device structure, and diffusion length as inputs and predicts the resulting field and gain characteristics. The RPL model incorporates a "triangular" electric field in the p$^+$ and n$^+$ regions. Ohio State's analytical model makes several simplifying assumptions to speed the calculation in a non-linear least squares analysis. This analytical model assumes that carrier diffusion can be ignored[32] and treats the electric field as a top-hat shaped function that extends into the p$^+$ and n$^+$ regions with increasing voltage. For this heterostructure, in which the p$^+$ and n$^+$ doping levels are 2×10^{18}, the depletion into the cladding regions is small compared to the avalanching width. Within these assumptions, Eqs. (3) and (4) can be combined and solved[8] to find the mean gain (M_a) as

$$M_a = \left(\frac{\gamma_\lambda}{e^{-\gamma_\lambda w} - 1}\right)\left[\frac{e^{\alpha w}(e^{-w(\alpha-\beta+\gamma_\lambda)} - 1)(\alpha - \beta)}{(\alpha e^{\beta w} - \beta e^{\alpha w})(\alpha - \beta + \gamma_\lambda)}\right]. \tag{5}$$

The analytical model parameterized w and E as

$$w = w_0 + w' \times V_{applied} = \frac{V_{applied} + V_{in-built}}{E}, \tag{6}$$

where w_0 is the depletion width at zero bias, w' is the slope of depletion width as a function of applied bias, V_{applied} is the applied bias, and $V_{\mathrm{in\text{-}built}}$ is the in-built bias. This parameterization is consistent with the measured CV data [Fig. 2(b)]. The w_0, w', and $V_{\mathrm{in\text{-}built}}$ coefficients for the analysis were obtained from a Silvaco model of the structure that was verified against the CV data. In both the RPL and analytical analyses, α and β are parameterized as[33]

$$\alpha = A_n e^{-\left(\frac{B_n}{E}\right)^{C_n}}, \tag{7}$$

$$\beta = A_p e^{-\left(\frac{B_p}{E}\right)^{C_p}}. \tag{8}$$

The six parameters—A_n, B_n, C_n, A_p, B_p, and C_p—are empirical parameters that are determined from the best fit to the gain data.

The input parameters for the two analyses are listed in Table I. The secondary ion mass spectrometry (SIMS) and CV measurements that support these parameters are shown in Fig. 2. The gain measurements indicate that 406 and 450 nm illumination resulted in single carrier injection, making gain independent of these absorption coefficients. For the other wavelengths, absorption coefficients measured using ellipsometry[12] were the starting point for the analysis. Both analyses found that the match between the gain measurements and predictions was improved by adjusting the absorption coefficients in the fit process, and the final coefficients agreed with the ellipsometry measurements within the experimental and analysis precision.

The two analysis approaches lead to similar assessments of α and β. Figure 3 shows the fit predictions and residuals for the two analyses, Table II compares the best-fit parameters, and Fig. 4 compares the predicted ionization coefficients. The predictions for α agree within $\pm$11% between breakdown and a gain of 2. The predictions for β agree within $\pm$50%, reflecting that the precision of β is poorer because it has less impact on the gain. The analytical fit estimates the precision of each parameter, and the relative precision of the A parameters indicates that the uncertainty in α is about $\pm$8% and the uncertainty in β is about $\pm$57%. The predicted parameterization for A_n, B_n, B_p, and C_n are similar, but A_p and C_p differ significantly. This parameter discrepancy is less significant than the ionization coefficient agreement. The C parameters have the least precision because of their correlation with A and B, and the analytical analysis could not estimate their precision. Caution should be used in assigning physical significance to these parameters, because C_n and C_p are predicted to be greater than one.

TABLE I. Input parameters for the Sheffield and Ohio State analyses of the gain data.

Input parameter	Value	Method
P-region thickness (nm)	300	SIMS
P-region doping (cm^{-3})	2×10^{18}	SIMS
I-region thickness (nm)	997	SIMS
I-region doping (cm^{-3})	1×10^{13}	Growth conditions
N-region thickness (nm)	100	SIMS
N-region doping (cm^{-3})	2×10^{18}	SIMS
w_0 (nm) [Eq. (6)]	999.95	Silvaco, SIMS, CV
w' (nm/V) [Eq. (6)]	0.320	Silvaco, CV
$V_{\mathrm{in\_built}}$ (V)	1.374	Silvaco
Diffusion length (μm)	0.1	RPL analysis

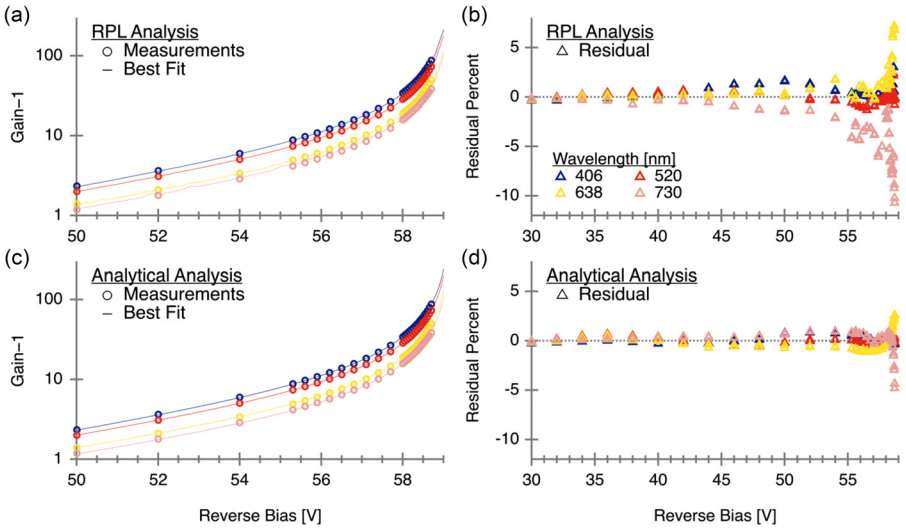

FIG. 3. (a) Comparison of measurements to the RPL best fit. (b) Fit residuals (measured−predicted)/measured, for the RPL best fit. (c) Comparison of measurements to the analytical best fit. (d) Fit residuals for the analytical best fit.

TABLE II. Ionization coefficient parameters for AlInAsSb obtained from the two analysis approaches. The parameters apply over the measured field range of 0.33–0.6 MV/cm The parameter precision estimates for the Analytical parameters are derived from the least squares fit. There were no reliable precision estimates for C_n or C_p due to their correlation with the corresponding A and B parameters.

Fit approach	A_n (10^3 cm^{-1})	B_n (10^3 V cm^{-1})	C_n	A_p (10^3 cm^{-1})	B_p (10^3 V cm^{-1})	C_p
RPL	180	790	2.3	1400	1800	1.68
Analytical	121 ± 10	708 ± 9	2.55	157 ± 89	1109 ± 74	2.29

Figure 4 compares the analyses for AlInAsSb to previously reported coefficients for AlAsSb,[36] InAlAs,[34] and AlGaAsSb[35] multipliers (all on an InP substrate). The AlInAsSb α is lower by a factor of 2–5 than these comparison materials, and β is lower than either InAlAs or AlGaAsSb. The differential between α and β, reflected in k, is comparable to AlGaAsSb but not as low as AlAsSb. This low k is promising for AlInAsSb to be able to achieve high gain with low excess noise. The excess noise for these AlInAsSb devices was measured by Sheffield using these same devices and while keeping the photon flux low to avoid gain suppression. The excess noise for 450 nm excitation is shown in Fig. 5 and compared to three predictions from local models. Below a gain of 10, the excess noise shows evidence of nonlocal behavior. Above a gain of 10, the excess noise increases linearly, consistent with a high-field k of approximately 0.044, a factor of 2 lower than the predictions from the ionization coefficient analysis. Lewis *et al.*[37] recently showed that the excess noise measured in AlGaAsSb is much lower than would be expected from the hole/electron ionization coefficient ratio, and a similar effect may be responsible for low noise in AlInAsSb. As shown in Fig. 5, the measured excess noise is significantly better than a commercially available SWIR InGaAs APD and is more like a Si APD. This excess noise is lower than InAlAs[21] at high gain, and it is lower than AlAsSb[38] and AlGaAsSb[26] up to a gain of ∼15 but then higher.

In conclusion, we presented the gain, ionization coefficients, and excess noise for the AlInAsSb alloy on an InP substrate, over a field

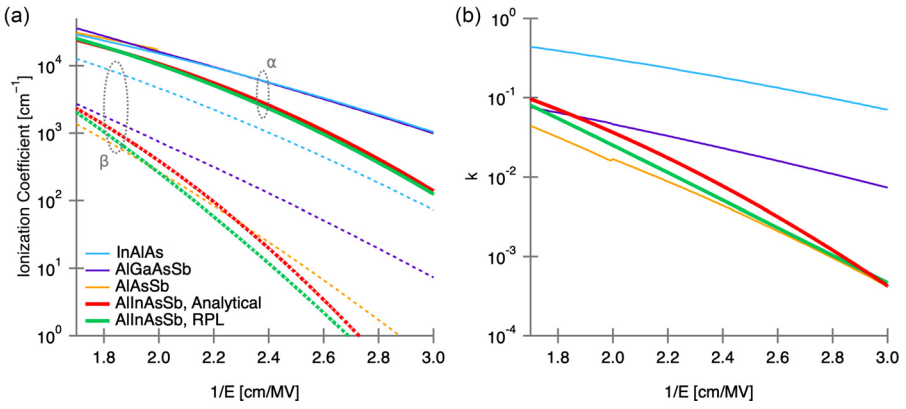

FIG. 4. (a) Experimental α and β coefficients vs inverse field for AlInAsSb (this report), InAlAs,[34] AlGaAsSb,[35] and AlAsSb.[36] (b) Calculated k for the same materials.

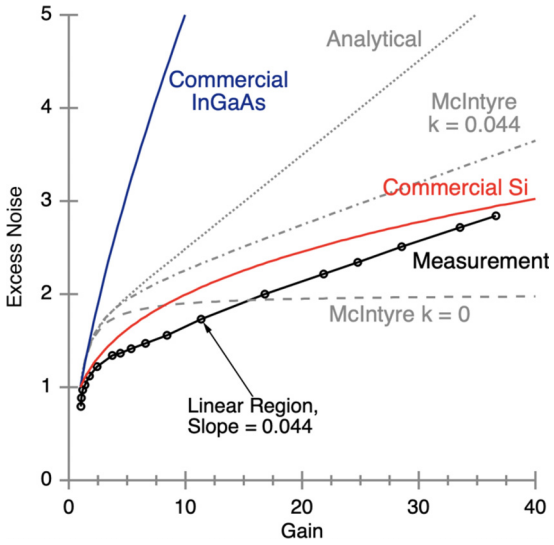

FIG. 5. Measured excess noise (F) vs gain (M) for a commercial SWIR InGaAs APD,[39] a commercial Si APD,[40] and this AlInAsSb. Three predictions of F vs M using the AlInAsSb Analytical analysis results[8] (with a varying k vs field) and McIntyre's excess noise formula.[7]

range of 0.33–0.6 MV/cm. These results will assist in the design and analysis of high-performance SWIR SACM APDs with an AlInAsSb multiplication layer on manufacturable InP substrates. The demonstrated characteristics are all improvements over a commercially available SWIR APD incorporating InGaAs as the multiplier.[39] The maximum demonstrated gain of 245 (a factor of 8 improvement), the relatively low dark current of 10^{-4} A/cm^2 (a factor of 10 improvement) at a gain of 30, and the low excess noise of 2.5 (a factor of 4 improvement) at a gain of 30 all demonstrate that this is a promising multiplier material for SWIR APD applications.

See the supplementary material for x-ray diffraction (XRD) data for the material, a comparison of the current–voltage characteristics of the previously and newly fabricated devices, and an analysis of dark current as a function of gain.

This work was supported by the Directed Energy–Joint Technology Office (DE-JTO), Award No. N00014-17-1-2440. P. Martyniuk contribution was supported by the National Science Centre (Poland), Grant Nos. UMO-2019/33/B/ST7/00614 and UMO-2021/41/B/ST7/01532. S. H. Kodati thanks Manisha Muduli for helpful discussions and testing during the fabrication of test devices.

AUTHOR DECLARATIONS

Conflict of Interest

The authors have no conflicts to disclose.

Author Contributions

T. J. Ronningen, S. H. Kodati, and X. Jin contributed equally to this work.

Theodore James Ronningen: Formal analysis (equal); Investigation (equal); Methodology (equal); Writing – original draft (equal). **Sri Harsha Kodati:** Conceptualization (lead); Formal analysis (equal); Investigation (equal); Methodology (lead); Writing – original draft (equal). **Xiao Jin:** Formal analysis (lead); Investigation (equal); Methodology (equal); Writing – original draft (equal). **Seunghyun Lee:** Formal analysis (supporting); Validation (lead); Writing – review & editing (supporting). **Hyemin Jung:** Investigation (supporting); Resources (equal). **Xiaofeng Tao:** Formal analysis (supporting); Investigation (supporting). **Harry Lewis:** Formal analysis (supporting); Methodology (supporting). **Mariah Schwartz:** Investigation (supporting). **Nathan Gajowski:** Investigation (supporting); Resources (supporting). **Piotr Martyniuk:** Investigation (supporting); Methodology (supporting); Resources (equal). **Bingtian Guo:** Investigation (supporting). **Andrew H. Jones:** Methodology (supporting); Resources (equal). **Joe C. Campbell:** Supervision (supporting); Writing – review & editing (supporting). **Christoph H. Grein:** Supervision (supporting); Writing – review & editing (supporting). **John P. R. David:** Supervision (supporting); Writing – review & editing (equal). **Sanjay Krishna:** Conceptualization (equal); Project administration (equal); Supervision (equal); Writing – review & editing (equal).

DATA AVAILABILITY

The data that support the findings of this study are available from the corresponding author upon reasonable request.

REFERENCES

[1]R. A. Barton-Grimley, A. R. Nehrir, S. A. Kooi, J. E. Collins, D. B. Harper, A. Notari, J. Lee, J. P. DiGangi, Y. Choi, and K. J. Davis, Atmos. Meas. Tech. **15**(15), 4623–4650 (2022).
[2]X. Sun, J. Abshire, M. Krainak, W. Lu, J. Beck, W. Sullivan, P. Mitra, D. Rawlings, R. Fields, D. Hinkley, and B. Hirasuna, Opt. Eng. **58**(6), 067103 (2019).
[3]Y. Li and J. Ibanez-Guzman, IEEE Signal Process. Mag. **37**(4), 50–61 (2020).
[4]C. P. Bradley, S. S. Mukherjee, A. D. Reinhardt, P. F. McManamon, A. O. Lee, and V. Dhulla, *Defense + Commercial Sensing* (SPIE, Baltimore, MD, 2019), Vol. 11005, p. 1100510.
[5]M. Kutila, P. Pyykönen, H. Holzhüter, M. Colomb, and P. Duthon, in *21st International Conference on Intelligent Transportation Systems (ITSC)* (IEEE, 2018), pp. 1695–1701.
[6]G. E. Stillman and C. M. Wolfe, in *Semiconductors and Semimetals*, edited by R. K. Willardson and A. R. Beer (Elsevier, 1977), pp. 291–393.
[7]R. J. McIntyre, IEEE Trans. Electron Devices **ED-13**(1), 164–168 (1966).
[8]M. M. Hossain, J. P. R. David, and M. M. Hayat, J. Lightwave Technol. **37**(13), 3315–3323 (2019).
[9]D. S. Ong, A. H. Tan, K. Y. Choo, K. H. Yeoh, and J. P. R. David, J. Phys. D **55**(6), 065105 (2022).
[10]R. J. McIntyre, IEEE Trans. Electron Devices **46**(8), 1623–1631 (1999).
[11]P. Yuan, K. Anselm, C. Hu, H. Nie, C. Lenox, A. Holmes, B. Streetman, J. Campbell, and R. McIntyre, IEEE Trans. Electron Devices **46**(8), 1632–1639 (1999).
[12]S. H. Kodati, S. Lee, B. Guo, A. H. Jones, M. Schwartz, M. Winslow, N. A. Pfiester, C. H. Grein, T. J. Ronningen, J. C. Campbell, and S. Krishna, Appl. Phys. Lett. **118**, 091101 (2021).
[13]W. Sullivan, J. Beck, R. Scritchfield, M. Skokan, P. Mitra, X. Sun, J. Abshire, D. Carpenter, and B. Lane, J. Electron. Mater. **44**(9), 3092–3101 (2015).
[14]Hamamatsu, *InGaAs APD, G14858* (Hamamatsu Photonics, 2019).
[15]N. Li, R. Sidhu, X. Li, F. Ma, X. Zheng, S. Wang, G. Karve, S. Demiguel, A. L. Holmes, and J. C. Campbell, Appl. Phys. Lett. **82**(13), 2175–2177 (2003).
[16]S. Hwang, J. Shim, and K. Yoo, J. Korean Phys. Soc. **49**(1), 253–260 (2006).
[17]Y. Zhao and S. He, Microelectron. Eng. **98**, 19–23 (2012).
[18]L. W. Cook, G. E. Bulman, and G. E. Stillman, Appl. Phys. Lett. **40**(7), 589–591 (1982).

[19]Y. Yuan, J. Zheng, Y. Tan, M. Ren, Y. Peng, A.-K. Rockwell, S. R. Bank, A. Ghosh, and J. C. Campbell, Photonics Res. **6**(8), 794–799 (2018).
[20]X. G. Zheng, J. Hsu, J. B. Hurst, X. Li, S. Wang, X. Sun, A. L. Holmes, J. C. Campbell, A. S. Huntington, and L. A. Coldren, IEEE J. Quantum Electron. **40**(8), 1068–1073 (2004).
[21]J. Zheng, Y. Yuan, Y. Tan, Y. Peng, A. K. Rockwell, S. R. Bank, A. W. Ghosh, and J. C. Campbell, J. Lightwave Technol. **36**(17), 3580–3585 (2018).
[22]D. S. G. Ong, J. S. Ng, Y. L. Goh, C. H. Tan, S. Zhang, and J. P. R. David, IEEE Trans. Electron Devices **58**(2), 486–489 (2011).
[23]J. Xie, S. Xie, R. C. Tozer, and C. H. Tan, IEEE Trans. Electron Devices **59**(5), 1475–1479 (2012).
[24]C. H. Tan, S. Xie, and J. Xie, IEEE J. Quantum Electron. **48**(1), 36–41 (2012).
[25]S. Lee, X. Jin, H. Jung, H. Lewis, Y. Liu, B. Guo, S. H. Kodati, M. Schwartz, C. H. Grein, T. J. Ronningen, J. P. R. David, J. C. Campbell, and S. Krishna, Optica **10**, 147–154 (2023).
[26]S. Lee, B. Guo, S. H. Kodati, H. Jung, M. Schwartz, A. H. Jones, M. Winslow, C. H. Grein, T. J. Ronningen, J. C. Campbell, and S. Krishna, Appl. Phys. Lett. **120**(7), 071101 (2022).
[27]S. Lee, S. H. Kodati, B. Guo, A. H. Jones, M. Schwartz, M. Winslow, C. H. Grein, T. J. Ronningen, J. C. Campbell, and S. Krishna, Appl. Phys. Lett. **118**, 081106 (2021).
[28]S. Lee, M. Winslow, C. H. Grein, S. H. Kodati, A. H. Jones, D. R. Fink, P. Das, M. M. Hayat, T. J. Ronningen, J. C. Campbell, and S. Krishna, Sci. Rep. **10**(1), 16735 (2020).
[29]S. H. Kodati, Ph.D. dissertation, The Ohio State University, 2022.
[30]M. Moresco, F. Bertazzi, and E. Bellotti, IEEE J. Quantum Electron. **47**(4), 447–454 (2011).
[31]D. S. Ong, K. F. Li, G. J. Rees, J. P. R. David, and P. N. Robson, J. Appl. Phys. **83**(6), 3426–3428 (1998).
[32]G. J. Rees and J. P. R. David, J. Phys. D **43**(24), 243001 (2010).
[33]P. Yuan, C. C. Hansing, K. A. Anselm, C. V. Lenox, H. Nie, A. L. Holmes, B. G. Streetman, and J. C. Campbell, IEEE J. Quantum Electron. **36**(2), 198–204 (2000).
[34]Y. L. Goh, D. J. Massey, A. R. J. Marshall, J. S. Ng, C. H. Tan, W. K. Ng, G. J. Rees, M. Hopkinson, J. P. R. David, and S. K. Jones, IEEE Trans. Electron Devices **54**(1), 11–16 (2007).
[35]B. Guo, X. Jin, S. Lee, S. Z. Ahmed, A. H. Jones, X. Xue, B. Liang, H. I. J. Lewis, S. H. Kodati, D. Chen, T. J. Ronningen, C. H. Grein, A. W. Ghosh, S. Krishna, J. P. R. David, and J. C. Campbell, J. Lightwave Technol. **40**(14), 4758–4764 (2022).
[36]X. Yi, S. Xie, B. Liang, L. W. Lim, X. Zhou, M. C. Debnath, D. L. Huffaker, C. H. Tan, and J. P. R. David, Sci. Rep. **8**(1), 9107 (2018).
[37]H. I. J. Lewis, X. Jin, B. Guo, S. Lee, H. Jung, S. H. Kodati, B. Liang, S. Krishna, D. S. Ong, J. C. Campbell, and J. P. R. David, Sci. Rep. **13**(1), 9936 (2023).
[38]X. Yi, S. Xie, B. Liang, L. W. Lim, J. S. Cheong, M. C. Debnath, D. L. Huffaker, C. H. Tan, and J. P. R. David, Nat. Photonics **13**, 683–686 (2019).
[39]Hamamatsu, *InGaAs APD, G8931* (Hamamatsu Photonics, 2019).
[40]Hamamatsu, *Si APD, S12023 Series* (Hamamatsu Photonics, 2022).